

國立交通大學

電機學院光電顯示科技產業研發班

碩士論文

四點探針有機薄膜電晶體之氣體感測研究

Study of Gas Sensing Ability on Gated-Four-Probes

Organic Thin Film Transistors

研究生：吳文馨

指導教授：冉曉雯 博士

中華民國九十六年八月

四點探針有機薄膜電晶體之氣體感測研究

Study of Gas Sensing Ability on Gated-Four-Probes

Organic Thin Film Transistors

研究生：吳文馨

Student：Wen-xin Wu

指導教授：冉曉雯

Advisor：Dr. Hsiao Wen Zan

國立交通大學

電機學院光電顯示科技產業研發碩士班



A Thesis

Submitted to College of Electrical and Computer Engineering

National Chiao Tung University

in partial Fulfillment of the Requirements

for the Degree of

Master

in

Industrial Technology R & D Master Program on

Photonics and Display Technologies

August 2007

Hsinchu, Taiwan, Republic of China

中華民國九十六年八月

四點探針有機薄膜電晶體之氣體感測研究

研究生：吳文馨

指導教授：冉曉雯 博士

國立交通大學

電機學院光電顯示科技產業研發碩士專班

摘 要

在論文中，我們建立一個可定量控制氣體濃度的感測系統，並利用具四點探針結構的有機薄膜電晶體進行氨氣感測的研究。當氨氣與有機薄膜電晶體反應時，電晶體的汲極電流會被減少、臨界電壓會往負值增加、但次臨界擺幅幾乎不受氨氣的影響而改變。而由四點探針結構的量測顯示，電晶體的薄膜電阻與接觸電阻均隨氨氣濃度的提高而增加。而利用薄膜電阻所推算出來的本質載子遷移率也會因氨氣濃度的提高而隨之減少。最後則將探討載子遷移率降低、臨界電壓往負值增加、及幾乎不受氨氣影響的次臨界擺幅，並根據電晶體特性改變的結果，提出可能的反應機制。

Gas sensing ability of Gated-Four-Probes OTFTs study

Student: Wen-xin Wu

Advisor: Dr. Hsiao-Wen Zan

Industrial Technology R & D Master Program of
Electrical and Computer Engineering College
National Chiao Tung University

Abstract

In this thesis, we tried to construct a gas sensing system, in which we can control the gas concentration quantitatively; moreover we also utilized the gated-four-probes organic thin film transistor to investigate the NH_3 gas-sensing experiment. When the NH_3 gas was interacted with OTFT, it was found that the OTFT drain current will be reduced and the threshold voltage will be enlarged toward a negative value. However, the subthreshold swing was not changed significantly by the NH_3 gas. From the analysis of gated-4-probes OTFT, both the film resistance and the contact resistance were increased with the raise of NH_3 concentration. Additionally, the intrinsic field-effect mobility, which was estimated from the film resistance, was also reduced with the raise of NH_3 concentration. Finally, the reduction of the mobility, the increase of the

threshold voltage, and the almost unchanged subthreshold swing were discussed.

A probable mechanism deduced from the change of the OTFT was also summarized and proposed in this study.



Acknowledgement

在這兩年的碩士班生涯期間，首先要感謝的是指導教授冉曉雯老師，老師在我的碩士班研究題目上給我的建議，和對於這個主題的未來展望，您悉心的教導使我得以一窺有機薄膜電晶體領域的深奧，不時的討論並指點我正確的方向，使我在這兩年中獲益匪淺。

本論文的完成另外亦得感謝生化工程研究所的楊裕雄教授在硬體上大力支持，及生化工程研究所羅淵仁和蕭程允學長的協助，提供我實驗上所需要的設備。因為有你們的體諒及幫忙，使得本論文能夠更完整而嚴謹。

感謝實驗室的學長們，在我對於研究上的一些疑惑，和你們討論後總是能激發我一些靈感，啟發我再去思考的動力。特別感謝國錫學長，總是不厭其煩的指出我研究中的缺失，並給予建議。也感謝實驗室的同學們：芸嘉、廷遠、高手、小七、睿志、光明、而康同學的幫忙，恭喜我們順利走過這兩年。實驗室的武衛、權陵、俊傑、志宇學弟、旻君學妹，你們幫忙我銘感在心。

最後，謝謝我的家人，感謝你們從小到大的支持與照顧！

吳文馨
2007 夏 于新竹

Contents

Chinese Abstract	i
English Abstract	ii
Acknowledgment	iv
Contents	v
Figure Captions	vii
Chapter 1	Introduction.....	1
1-1	Introduction of organic thin film transistors (OTFTs)	1
1-2	Applications of OTFTs to gas-sensing device.....	2
1-3	Objective and Motivation.....	2
1-4	Organization of thesis.....	3
Chapter 2	Theoretical background of OTFTs.....	5
2-1	Transportation mechanisms of organic semiconductor.....	5
2-2	Interaction of gases on OTFTs.....	7
2-3	Potential Effects on Gas Sensing in OTFT.....	8
2-3.1	Morphology and dimension of Active Layer.....	8
2-3.2	Dipole of the analyte.....	9
2-3.3	The Thickness of Active Layer.....	9
2-3.4	Device area.....	9

2-4	Gated four-probes OTFTs for resistance measurement.....	10
CHAPTER 3	EXPERIMENT	13
3-1	Device Fabrication.....	13
3-1.1	Preparation of Substrates.....	13
3-1.2	Spin-coated PMMA on SiO ₂	13
3-1.3	Growth of Thin Film and Electrodes.....	14
3-2	Gas sensing system.....	14
CHAPTER 4	Result and Discussion	16
4-1	Characteristics of Gated-Four-Probes OTFTs.....	16
4-2	Effects of ammonia (NH ₃) on Gated four-probe OTFTs.....	18
CHAPTER 5	Conclusion	23
REFERENCE	24

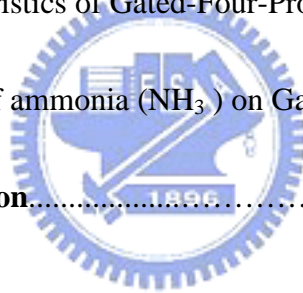


Figure Captions

Chapter 1

Figure 1.1 The applications of plastic transistors: (a) flexible displays, (b) smart cards, (c) RFID tags, and (d) the nervous system of robot skin.

Figure 1.2 Evolution of hole mobility for the most common p-type organic semiconductors.

Chapter 2

Figure 2.1 The degradation of field-effect mobility from two OTFTs with different channel dimensions.

Figure 2.2 (a) Top view of a gated-four-probes OTFT. (b) The potential distribution in an OTFT channel region. The potential drop of the organic film is assumed to be linear. But the potential different at the source and drain electrodes are also given.

Figure 2.3 The voltage difference between two voltage probes $V_1 - V_2$ are plotted as a function of drain voltage at different gate voltage.

Chapter 3

Figure 3.1 Diagram of gas sensing measurement system

Figure 3.2 The mass flow controller of gas sensing system. (b) The power supply of mass flow controller. (c) The pressure gauge of gas sensing system.

Figure 3.3 Top-view image of gas-sensing system.

Figure 3.4 Top-view image of gas-sensing system mounting a metal cap with transparent window.

Chapter 4

Figure 4.1 The atomic force microscope (AFM) images of (a) SiO₂ dielectric. (b) PMMA-coated SiO₂ dielectric. (c) pentacene AFM image on PMMA-coated SiO₂ layer.

Figure 4.1 The drain-current is plotted as a function of gate-voltage. (a) Device is operated at linear region. (b) Device is operated at saturation region.

Figure 4.3 (a) The voltage difference between potential-probes is plotted as a function of drain voltage, at different gate voltage respectively. (b) The output characteristics ($I_D - V_D$) show that when V_D increases, the $I_D - V_D$ curve will be converted from a linear-relation to a saturated-relation.

Figure 4.4 The transfer characteristic of gate-four-probes OTFT is plotted in (a) semi-log scale and (b) linear-scale, respectively.

Figure 4.5 The total contact resistance (R_{cont}) and the pentacene film resistance (R_{film}) is plotted as a function of gate-voltage minus threshold-voltage ($V_G - V_{th}$), respectively.

Figure 4.6 (a) The R_{cont} and R_{film} is further plotted as a function of NH₃ concentration. (b) The percentage (%) of R_{cont} and R_{film} versus NH₃ concentration.

Figure 4.7 4-7 The extracted ontrinsic field-effect mobility is plotted as a function of NH₃ concentration gas at a $V_D = -3V$ and $V_G - V_{th} = -25V$.

Figure 4.8 4-8 (a) The threshold voltage shift (ΔV_{th}) and (b) the subthreshold swing ($S.S.$) is also plotted as a function of NH_3 concentration, respectively.

Figure 4.9 4-9 The estimated GB barrier height and GB trap density is plotted as a function of NH_3 concentration.

Figure 4.10 4-10 The subthreshold swing and interface trap density will not be influenced significantly after the pentacene film interacts with the NH_3 molecular.



CHAPTER 1

Introduction

1.1 Introduction of organic thin film transistors (OTFTs)

“Plastic transistors” open the future of flexible displays, smart cards, radio frequency (RF) identification tags, as well as light-emitting diodes (LED) and lasers [1]. Rapid progress in this field has been achieved by improving the material properties and the process techniques .

As for the application of electronics, the organic active layer has attained a mobility of $1\text{cm}^2/\text{Vs}$ and a switching speed of 10^8 Hz, which is comparable to amorphous hydrogenated silicon (a-Si:H) , as shown in Fig. 2.1 [2]. Since the late 1940s, there has been a lot of research on the development of organic semiconductor [3]. This is because of the large π -conjugation length along the long axis of the molecules and closed π -stacking are the key factors of high carrier mobility [3].

Similar to inorganic semiconductors, organic ones can function as p-type or n-type. However, most reported high-mobility organic semiconductors are p-type material. Among the p-type material, pentacene ($\text{C}_{14}\text{H}_{22}$), a rod-like aromatic molecule composed of five benzene rings, shows the highest mobility ($>1\text{cm}^2/\text{Vs}$), owing to highly ordered films with proper dielectric properties and growth conditions [4].

1.2 Applications of OTFTs to gas-sensing device

For the next generation of sensor applications on medical diagnostics, food monitoring, and chemical or biological warfare etc.; portable, low cost, and low power-consumption will be important demands. As for these demands, the OTFT should be an important candidate due to its flexibility and its simple fabrication process. Therefore, the studies of organic thin-film transistors (OTFTs) to physical, chemical, and biological sensors will become an important object [5,6,7,8].

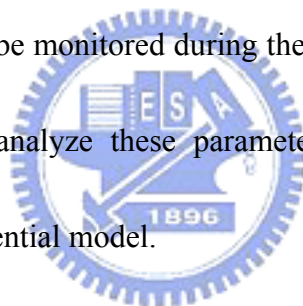
Recently, OTFTs are proposed to act as gas sensors. When OTFTs exposed to gaseous species, five parameters: such as the turn-on current (I_{on}), turn-off current (I_{off}), threshold-voltage (V_{th}), field-effect mobility (μ_{eff}) and subthreshold-swing ($S.S.$), are used to estimate the gaseous interaction in OTFTs. By this way, a “multi-parameter” gas sensor can be realized by OTFT [9].

1.3 Objective and Motivation

Although the primary gaseous interactions on OTFTs are observed, however, the details of mechanisms are still not well-understood. Unlike the inorganic materials, the bindings between the organic molecules are weak van der Waal force. The stack of organic crystal is loose and contained with voids. Therefore, the gas penetration and gas interaction to the organic devices will be strongly dominated by the organic

semiconductor layer. Besides, the loosely packed organic-film with aromatic compounds will be a good medium for bio-molecules. As a result, to investigate the fundamental of gaseous and biochemical interaction on OTFTs should open a road to high-sensitive organic sensors.

In this study, we try to investigate the effect of sensing ammonia(NH_3) in pentacene-based OTFTs. By the gated-4-probes OTFTs, the organic film properties and metal-contact effects can be studied separately. The related parameters of TFT, such as pentacene film resistances, intrinsic mobility, threshold voltage, and the subthreshold swing, will also be monitored during the gaseous experiment on OTFTs. Afterwards, we will try to analyze these parameters to characterize the sensing mechanism and propose a potential model.



1.4 Organization of thesis

In chapter 1, we make a brief introduction to the demands on OTFTs and its application on gas sensing. Consequently, in chapter 2, we discuss some basic knowledge about the device operations and the gas sensing properties in OTFTs. The studies of gated-4-probes OTFTs and its analysis are also presented in this part. In chapter 3, the experimental details, such as the devices fabrication, and the connection of gas sensing system are discussed. The effect of sensing ammonia(NH_3) on OTFT is presented in chapter 4. The transfer characteristics will be shown in

these chapters. The related OTFT parameters will also analyze under different gas concentration. In final chapter, we will make a conclusion.



CHAPTER 2

Theoretical background of OTFTs

2-1 Transportation mechanisms of organic semiconductor

In the past 20 years, a great deal of progress has been made in improving the field-effect mobilities of OFETs [10,11]. It has also been demonstrated that the properties of charge transport in conjugated molecules are intrinsically correlated with their crystalline structure, where the π delocalized carriers are responsible for the intra-molecular conduction. However, the nature of van der Waals bonding between discreted molecules is thought to be a limitation of the carrier transport, and the transport is usually described by “localized model” [3]. Thus, the charged carrier transport must be described by different models than those in covalently bonded semiconductors.

Recently, two principal types of theoretical models are used to describe the transport in organic semiconductors : “The band-transport model” and “The hopping models”. However, band transport may not suit for some disordered organic semiconductors, in which carrier transport is govern by the hopping between localized states. Hopping is assisted by phonons and the mobility increases with temperature. Typically, the mobility is very low, usually much lower than $1\text{cm}^2/\text{V}\cdot\text{sec}$. The boundary between “band transport” and “hopping” is divided by materials mobilities

($\sim 1\text{cm}^2/\text{V}\cdot\text{sec}$) at room-temperature (RT) [12]. Many kinds of polycrystalline organic semiconductors, such as several members of the acene series including pentacene, rubrene, have RT mobility over the boundary [13]. Sometimes, temperature-independent mobility was found in some polycrystalline pentacene devices [14]. Thus, this observation argued that the simply thermal activated hopping process governed the whole carrier transport behaviors in high quality polycrystalline pentacene film, despite that the temperature independent mobility has been observed in exceptional cases [14].

The understanding of carrier transport in single-crystal of organic semiconductors will help us to describe the transport mechanism in polycrystalline organic semiconductors. The coherent band-like transport of delocalized carriers becomes the prevalent transport-mechanism in the single crystal organic semiconductors, such as pentacene, tetracene, under the low-temperature environments. A very high hole mobility has been measured by time-of-flight (TOF) experiments [15]. Thus, the temperature dependence of the carrier mobility was found below 100K and following with a power law of $\mu \propto T^{-n}$, $n \sim 1$ [16], in single crystals of organic semiconductors, consistent with the band-transport model. However, between 100K and 300K, the carrier mobility show a constant value [16], that has been described as the superposition of two independent carrier transport

mechanisms. The first mechanism was small molecular polaron (MP). According to this model, the carriers were treated as the heavy, polaron-type, and quasi-particles. It is formed by the interaction of the carriers with intra-molecular vibrations of the local lattice environment, and move coherently via tunneling. In this model, the mobility follows the power law $\mu_{MP}=aT^{-n}$. The other involves a small lattice polaron (LP), which moves by thermally activated hopping and exhibits a typical exponential dependence of mobility on temperature : $\mu_{LP}=b\exp[-Ea/kT]$. The superposition of these two mechanisms could get a good consistence with experimental measurement of temperature-dependence mobility from room temperature to a Kelvin degrees (K) [17].



2-2 Interaction of gases on OTFTs


The OTFTs gas sensing have been several advantages over the chemical resisters. These devices are especially attracted due to their ability to serve as a multi-parameter sensor [9].

Furthermore, Frank Liao indicated that there is the potential for discrimination based on the functional group chemistry of the analytics. The presence of π orbitals or the acidic proton in the acetic acid interacts with the channel of the device to cause trapping and decrease the mobility [7].

2-3 Potential Effects on Gas Sensing in OTFT

2-3.1 Morphology and dimension of Active Layer

Grain boundaries (GBs) play a critical role in OFET sensing. In the reported researches, the control of grain size can be achieved by changing the substrate temperature during deposition. According to the images of transmission electron microscope (TEM), Torsi *et al.* indicate that the response is strong for the low-temperature film, which has more grain boundaries. However, the response is weak for the high-temperature film, which has fewer grain boundaries and shows a more compacted structure [18].




Wang *et al.* also indicate that device channel scale being an important key in sensing process with different mechanisms dominating at different length scales. For a longer channel relative to grain sizes, there are enough grain boundaries inside the channel so that the former effect is dominant and the overall sensing response is the current decreasing. For a shorter channel relative to grain sizes, the latter effect dominates due to very few number of grain boundaries inside channel, which leads to the current increasing by excess charges from the interaction between grains and the analyte [19].

2-3.2 Dipole of the analyte

For the most analytes, the interactions are attributed to the nature of molecular dipole. For example, the H₂O will result in the decrease of drain-current [20,21]. Although pentacene is highly hydrophobic, H₂O molecules can easily diffuse into these devices, interact with the traps by and alter the electric field at the grain boundaries. In addition, the presence of polarized molecules is known to decrease the rate of charge transport in organic materials by increasing the amount of energetic disorder through charge–dipole interactions [20].

2-3.3 The Thickness of Active Layer



Yang *et al.* indicate that ultrathin cobalt phthalocyanine (CoPc) transistors of 4 ML compare faster response times, higher base line stabilities, and more sensitive to 50 ML devices [22]. Due to the ultrathin ChemFETs, the holes accumulation extends to the air/CoPc interface; therefore, the surface traps participate in carrier transport and the perturbation of the surface trap energies by the analytes renders the ultrathin ChemFETs more sensitive than the thick ChemFETs [22].

2-3.4 Device area

F. Liao *et al.* indicated that the device area does not affect the overall sensor

response. Different device areas of $(W/L)_1 = 500/25$ and $(W/L)_2 = 100/4$ both show the same percent change in active current [7].

But in our gas sensing experiments from different dimension of OTFT are show in Fig. 2.1. Different size OTFT will show a slightly different response.

2-4 Gated four-probes OTFTs for resistance measurement

Gated four-probe OTFTs measurements were carried out by using a Keithley 4200-SCS semiconductor parameter analyzer. In the four-terminal measurements, as

show in Fig. 2-2(a) the voltage V_1 and V_2 between the source and drain electrodes.

The probing current of voltage probes is about 10^{-13} A, which is lower than the drain-current. In Fig. 2-2(b), an idealized depiction of the potential distribution in the

channel region, when OTFT is operated in linear region and above threshold condition $|V_{DS}| < |V_{GS} - V_T|$. Where V_T is the threshold voltage, V_{GS} is the

gate-source voltage, and V_{DS} is the drain-source voltage. In Fig. 2-3, the voltage

difference between the voltage probes $V_1 - V_2$ from four-terminal measurement. This

voltage difference varies linearly with increasing V_{DS} over a limited range of V_{DS}

and shows almost no gate voltage dependence. Such linear dependence on V_{DS} is

expected if the device behaves as predicted by simple FET theory. At a large V_{DS} , the

potential difference between the voltage probes is nearly constant and independent of

V_{DS} . This behavior is also predicted from simple FET theory for the saturation region.

By measuring, V_1 and V_2 , a linear extrapolation of the potential profile to each contact was performed. The potential drops at the source electrode (ΔV_S), drain electrode (ΔV_D) and organic film (ΔV_{Film}), were calculated according to the following equations:

$$\Delta V_S = \left[V_2 - \frac{(V_1 - V_2)}{(L_2 - L_1)} (L - L_2) \right] - V_S \quad (1)$$

$$\Delta V_D = V_D - \left[V_2 + \frac{(V_1 - V_2)}{(L_2 - L_1)} L_2 \right] \quad (2)$$

$$\Delta V_{Film} = \frac{(V_1 - V_2)}{(L_2 - L_1)} L \quad (3)$$

where V_S , V_D , V_1 , and V_2 are the voltages at the source, drain, and two potential probes, respectively. L_1 is drain electrode to the first potential probe. L_2 is drain electrode to the second potential probe. L is the distances from the drain electrode to source electrode. Where ΔV_{Film} is the actual voltage drop across the film.

With the measured total current flowing through the device and the potential drops across the film and contacts, the resistance of the source contact, drain contact, and the film can be calculated using Ohm's Law, when devices operation in linear region.

$$R_S = \frac{\Delta V_S}{I_D} \quad (4)$$

$$R_D = \frac{\Delta V_D}{I_D} \quad (5)$$

$$R_F = \frac{\Delta V_F}{I_D} \quad (6)$$



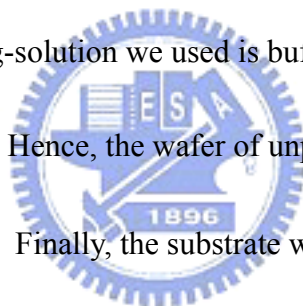
CHAPTER 3

EXPERIMENT

3.1 Device Fabrication

3.1-1 Preparation of Substrates

In this study, the OTFT devices we used are top-contact structures. A p-type, single crystal silicon wafer (100) was used as the substrate and the gate electrode. After RCA cleaning, a 1000Å thermally-grown SiO₂ layer was deposited on wafer by furnace. After the SiO₂ deposition, we removed the SiO₂ layer from the wafer of unpolished-side. The etching-solution we used is buffered oxide etching (B.O.E.) solution (NH₄F : HF=6 : 1). Hence, the wafer of unpolished-side without SiO₂ layer can serve as a gate-electrode. Finally, the substrate was cleaned in ultrasonic tank by the sequence of: de-ionic water (5 minutes), acetone (1 minutes), and de-ionic water (5 minutes).



3.1-2 Spin-coated PMMA on SiO₂

After substrate cleaning, we spun the solution-based Polymethylmethacrylate (PMMA) onto the substrate. The content of solution-based PMMA is a mix of PMMA and anisole with a concentration of 11.81wt%.

Consequently, we try to remove the residual solvent, by baking the substrate on hot-plate at 90°C about 30 minutes.

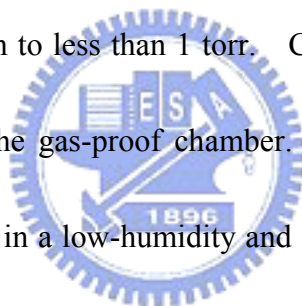
3.1-3 Growth of Thin Film and Electrodes

Pentacene powder was purchased from SIGMA-ALDRICH. Without any purification, pentacene powder was sublimated and deposited on substrate as an active layer under a pressure below 1.5×10^{-6} torr. The substrate was kept at 26°C. The deposition rate was about 0.5 Å/s and the pentacene-film thickness was about 1000 Å. All the deposition parameters are monitored by a quartz crystal microbalance (QCM) during the deposition process. In the end, a 1000 Å Au layer was used as the source and drain pad, which is deposited at a rate of 1~2 Å/sec under 3×10^{-6} torr. The channel width (W) and length (L) defined by shadow-mask was 800 μm and 1200 μm, respectively.

3.2 Gas-Sensing system

As shown in Fig. 3.1, the gas-sensing system consists of three major parts: a gaseous analyte controller, a gas-proof chamber, and a semiconductor parameter analyzer. In Fig. 3.2(a), (b), and (c), we show the mass flow controller, the power supply, and pressure gauge, respectively. The gaseous analyte was introduced into

the gas-proof chamber and controlled by the mass flow controllers (MFC; 5850E, Brooks Instrument). The pressure inside the gas-proof chamber was monitored by vacuum gauge (PC-615, PROTEC). The total volume of the gas-proof chamber is about 52.8 liter. Fig. 3.3 is the top-view image of gas-sensing system. The system was equipped with five Kelvin-probes and positioners. The probes were connected to the semiconductor analyzer (Keithley 4200-SCS) via tri-axial cables. The bottom pipe and the upper pipe served as the gas-inlet and gas-exhaust, respectively. After mounting a metal cap with transparent window, as shown in Fig. 3.4, the gas-proof chamber can be pumped down to less than 1 torr. Consequently, we introduced the pure nitrogen (N_2) gas into the gas-proof chamber. Thus, all the gaseous-sensing experiments can be processed in a low-humidity and low-oxygen ambiance. All the experiments were also be operated at a pressure about 760 torr.



CHAPTER 4

Result and Discussion

4-1 Characteristics of Gated-Four-Probes OTFTs

In order to improve the OTFTs performance and pentacene crystallization, the SiO₂ surface is spin-coated with an ultra-thin PMMA layer. In Fig. 4-1(a) and (b), we show the atomic force microscope (AFM) images of SiO₂ dielectric and PMMA-coated SiO₂ dielectric. As we can observe, the surface roughness of SiO₂ and PMMA-coated SiO₂ is about 0.21 nm and 0.20 nm, respectively. The PMMA layer will not affect the surface roughness significantly. From the capacitance measurements, the total capacitance value is reduced from 34 nF/cm² to 23.4 nF/cm². By the serious-capacitance formula:

$$\frac{1}{C_{total}} = \frac{1}{C_{SiO_2}} + \frac{1}{C_{PMMA}}$$

$$C_i = \frac{\epsilon_0 \cdot \epsilon_i}{t_i}$$

C_{total} , C_{SiO_2} , and C_{PMMA} is the total capacitance, the SiO₂ capacitance, and the PMMA capacitance, respectively. ϵ_0 is the permittivity in vacuum. ϵ_i and t_i indicates the relative dielectric constant and the dielectric thickness, respectively.

By taking the $\epsilon_{SiO_2} = 3.9$, $t_{SiO_2} = 100nm$, and $\epsilon_{PMMA} = 3.5$, the estimated thickness of PMMA layer is about 41 nm. The pentacene AFM image on PMMA-coated SiO₂

layer is also shown in Fig. 4-1(c), an average grain-size and roughness about $1\sim 2 \mu m$ and 15.1 nm can be observed in the figure, respectively. After the source, drain, and voltage-probing electrodes are deposited on pentacene film, we measured the transfer characteristics of the gated-4-probes OTFT. The drain-current is plotted as a function of gate-voltage in Fig. 4-2. The device shows an on/off current ratio about 5 orders and a low hysteresis when the device is operated above the threshold voltage.

To obtain correct parameters from gated-4-probes OTFT, it is important to choose the range of operation voltage. It is well known that four-terminal electrical measurement is based on Ohm's Law. The voltage-drop will be linearly changed with the increase of drain-voltage. However, the linear-dependence is not always expected at any voltage bias. As shown in Fig. 4-3 (a), the voltage difference between potential-probes is plotted as a function of drain voltage, respectively. The voltage difference ($V_2 - V_1$), will not linearly increase with drain-voltage (V_D) and show almost no gate-voltage (V_G) dependence when the V_D is less than -4 V . The result can be explained by the output characteristics ($I_D - V_D$) in Fig. 4-3(b). When the V_D increases, the $I_D - V_D$ curve is converted from a linear-relation to a saturated-relation. It is clear that when the gated-4-probes OTFT is operated at a small V_D e.g. less than -5 V , the extracted parameters will be correct. Hence, in the consequent experiment, the V_D is fixed at -3 V .

4-2 Effects of ammonia (NH₃) on Gated four-probe OTFTs

Before the measurement, the gas-sensing chamber is pumped-down to less than 1 torr and vented to 760 torr by the high-purity nitrogen (N₂) gas. Initially, we measured the gated-4-probe OTFT in the nitrogen ambience. As shown in Fig. 4-4(a) and 4-4(b), the transfer characteristic is plotted in semi-log scale and linear-scale. Under the nitrogen ambience, the device show a mobility about 0.37 cm²/V-sec, an on/off current ratio more than 5 orders, a threshold voltage about -24 V, and a subthreshold swing about 0.97 decade/V. When the NH₃ is introduced into the chamber, the drain-current (I_D) will reduced with the increase of the NH₃ concentration. Interestingly, the threshold voltage will also shift more negatively. The on/off current ratio and the subthreshold swing will not be changed significantly with the increase of the NH₃ concentration.

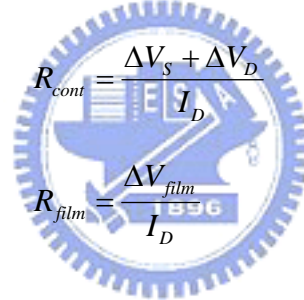
To further study the effects of NH₃ gas on OTFT devices, we try to estimate the contact resistance and pentacene resistance by the gated-4-probe OTFT, respectively. From potential-probes on channel, the voltage-drops at the source electrode (ΔV_s), drain electrode (ΔV_D), and within the pentacene film (ΔV_{film}) can be estimated by:

$$\Delta V_s = \left[V_2 - \frac{(V_1 - V_2)}{(L_2 - L_1)} (L - L_2) \right] - V_s$$

$$\Delta V_D = V_D - \left[V_2 + \frac{(V_1 - V_2)}{(L_2 - L_1)} L_2 \right]$$

$$\Delta V_{Film} = \frac{(V_1 - V_2)}{(L_2 - L_1)} L$$

V_1 and V_2 is the voltage measured from the first potential probe (near the drain electrode) and second potential probe (near the source electrode), respectively. L_1 and L_2 is the distance from the first potential probe to drain electrode and the second potential probe to source electrode. L is the channel length. V_D and V_S is the drain voltage and source voltage, respectively. The total contact resistance (R_{cont}) and film resistance (R_{film}) can also be estimate by:



$$R_{cont} = \frac{\Delta V_S + \Delta V_D}{I_D}$$

$$R_{film} = \frac{\Delta V_{film}}{I_D}$$

As shown in Fig. 4-5, the R_{cont} and the R_{film} is plotted as a function of gate-voltage minus threshold-voltage ($V_G - V_{th}$), respectively. When the NH_3 gas is introduce into the gas-sensing chamber, both the R_{cont} and the R_{film} will increase. The R_{cont} and R_{film} is further plotted as a function of injected NH_3 in Fig 4-6(a). When the injected NH_3 is increased to 0.59 ppm, the R_{cont} will approach a maximum value about $1.0 \times 10^6 \Omega$, which is smaller than the value of R_{film} around $8.3 \times 10^6 \Omega$. The Fig. 4-6(b) shows the percentage (%) of R_{cont} and R_{film} versus injected NH_3 , respectively. It is clear that the percentage (%) of R_{film} is as high as about 90%

during the NH₃ gaseous experiment. Thus, the OTFT characteristics should be mainly dominated by the pentacene film properties rather than the contact properties.

Since the pentacene film properties will dominate the OTFT characteristics during the NH₃ gaseous experiment, we try to observe the intrinsic variation of field-effect mobility. In gated-4-probes measurement, the contact-corrected field-effect mobility (μ_{eff}) can be extracted by

$$\mu_{eff} = \frac{1}{C_{total}} \cdot \frac{\partial \sigma}{\partial V_G}$$

$$\sigma = \frac{I_D}{V_2 - V_1} \cdot \frac{L'}{W}$$

where C_{total} is the total capacitance of OTFT, σ is the conductivity, V_1 and V_2 is the voltage measured from the first potential probe (near the drain electrode) and second potential probe (near the source electrode), L' is the distance between two potential probes, and W is the channel width. The extracted contact-corrected field-effect mobility is plotted as a function of injected NH₃ gas at a $V_D = -3V$ and $V_G - V_{th} = -25V$ in Fig. 4-7. When the NH₃ concentration is increased, the contact-corrected field-effect mobility will decrease monochromatically from 0.39 $cm^2/V\text{-sec}$ to 0.34 $cm^2/V\text{-sec}$. The threshold voltage shift (ΔV_{th}) and the subthreshold swing ($S.S.$) is also plotted as a function of NH₃ concentration in Fig. 4-8(a) and Fig. 4-8(b), respectively. The threshold voltage will shift toward more negatively with the increase of NH₃ concentration. However, the subthreshold swing is kept at an

averaged value around 0.94 ± 0.03 *V/decade* and seems not be effected by the NH_3 dramatically, even when the NH_3 concentration is approached to a concentration of 0.59 ppm.

In none-crystalline semiconductor, the carrier field-effect mobility will be influenced by the grain-boundary (GB) potential barrier height $q\phi_b$. The mostly proposed GB barrier height model is described by

$$\mu_{eff} = \mu_{ig} \cdot \exp\left(-\frac{q\phi_b}{kT}\right)$$

$$\phi_b = \frac{qN_t^2 d}{8\epsilon_s C_{ox} (V_G - V_{th})}$$

Where μ_{ig} is intra-grain carrier mobility, q is elementary electron, N_t is the grain-boundary trap density, d is the thickness of semiconductor, ϵ_s is the semiconductor dielectric constant, C_{ox} is the gate insulator capacitance, k is the Boltzmann's constant, and T is the absolute temperature. According to the equation, the estimated GB barrier height and trap density is plotted as a function of NH_3 concentration in Fig. 4-9. As we can observe, the GB barrier height will slightly increase from 82.8 meV to 87.2 meV and the corresponding trap density will increase from 1.3×10^{11} to 1.4×10^{11} cm^{-2} , when the NH_3 is introduced into the chamber. Base on the experimental result, the reduction of drain current should be dominated by the slightly increased GB barrier. When the NH_3 molecular is introduced, the molecular will be adsorbed by the pentacene film. The polycrystalline pentacene

with a lot of GBs will serve additional sites to interact with NH₃ molecular. Hence, the absorbed NH₃ molecular on the GBs will increase the barrier height and acts as trapping sites.

It has also been reported that the amino function-groups will shift the OTFT threshold voltage and the turn-on voltage [24]. In our experiment, as shown in Fig. 4-8(a), an increased (negatively shift) threshold voltage implies the concentration of mobile holes in the pentacene film will be reduced. The NH₃ molecular shows the character of “hole-withdrawing” when it interacts with the pentacene film. It should attribute to the NH₃ molecular is polarized, which probably acts as a positive charged sites when it interacts with pentacene film. On the other hand, the interface trap density between the pentacene and dielectric can also be extracted from the subthreshold swing by

$$N_{ss} = \left[\frac{S \cdot \log(e)}{kT/q} - 1 \right] \cdot \frac{C_i}{q}$$

where S is the subthreshold swing; C_i is the capacitance per unit area; k is Boltzmann’s constant, and T is the absolute temperature. In Fig. 4-10, by substituting C_i =23.4 nf/cm² and S= 0.94±0.03V/decade yields an averaged interface trap density in the devices of 2.1×10¹² cm⁻²eV⁻¹. The interface trap density will not be influenced significantly after the pentacene film interacts with the NH₃ molecular.

CHAPTER 5

Conclusion

In summary, we constructed a gas-sensing system and investigated the interaction of pentacene film to NH_3 gas via the gated-4-probes OTFT. In our observation, when NH_3 gas interacted with the OTFT, both the contact resistance and the pentacene film resistance are increased, which resulted in the reduction of drain-current. The threshold voltage is also shifted negatively to a larger value; however, the subthreshold swing was almost unchanged. According to our estimation, the increase of pentacene-film resistance will reduce the intrinsic field-effect mobility. It should be attributed to the interaction of NH_3 gas and pentacene film will create additional traps in the pentacene grain, which will increase of grain boundary (GB) barrier height. On the other hand, based on the negatively increased threshold voltage and the almost unchanged subthreshold swing, the NH_3 shows a character of “hole withdrawing” in pentacene film but do not influence the distribution of interface trap significantly. We suggest that the strong interaction between NH_3 gas and OTFT may be connected to the highly polarized NH_3 molecule, but further work is needed to determine the detail of related mechanism.

REFERENCE

- [1] Frank-J. Meyer zu Heringdorf, M. C. Reuter and R. M. Tromp, "Growth dynamics of pentacene thin films," *Nature* **412**, pp.517 (2001).
- [2] Mattheus, Christine Corinne, "Polymorphism and Electronic Properties of Pentacene" (2002).
- [3] C. D. Dimitrakopoulos, and Patrick R. L. Malenfant, "Organic thin film transistors for large area electronics," *Adv. Mater.* **14**(2), pp.109 (2002).
- [4] D. Knipp, R. A. Street, A. Völkel, and J. Ho, "Pentacene thin film transistors on inorganic dielectrics: Morphology, structural properties, and electronic transport," *J. Appl. Phys.* **93**(1), pp.347 (2003).
- [5] Jeffrey T. Mabeck A George G. Malliaras, "Chemical and biological sensors based on organic thin-film transistors," *Anal Bioanal Chem* vol. **384**, pp. 343, (2006).
- [6] Jason Locklin . Zhenan Bao, "Effect of morphology on organic thin film transistor sensors," *Anal Bioanal Chem* vol. **384**, pp. 336, (2006).
- [7] Frank Liao, Christopher Chen, Vivek Subramanian, "Organic TFTs as gas sensors for electronic nose applications", *Sensors and Actuators B*, vol.107, pp.**849**, (2005)
- [8] I. Manunza, A. Bonfiglio, "Pressure sensing using a completely flexible organic transistor," *Biosensors and Bioelectronics*, vol.**22**, pp.2775 (2007)
- [9] L. Torsi, A. Dodabalapur, L. Sabbatini, P.G. Zambonin, "Multi-parameter gas sensors based on organic thin-film-transistors," *Sensors and Actuators B*, vol.**67**,

pp.312, (2000)

- [10] A. Tsumura, K. Koezuka, and T. Ando, “Macromolecular electronic devices: Field-effect transistor with a polythiophene thin film”, *Appl. Phys. Lett.* vol.**49**, pp. 1210, (1986).
- [11] J. H. Burroughes, C. A. Jones, and R. H. Friend, “Polymer diodes and transistors: new semiconductor device physics”, *Nature*, vol. **335**, pp.137, (1988).
- [12] G. Horowitz, “Organic field-effect transistors”, *Adv. Mater.*, vol. **10**, pp. 365, (1998).
- [13] Y.-Y. Lin, D. J. Gundlach, S. F. Nelson, and T. N. Jackson, “Stacked pentacene layer organic thin-film transistors with improved characteristics”, *IEEE Electron Device Lett*, vol. **18**, pp 606, (2000).
- [14] S. F. Nelson, Y.-Y. Lin, D. J. Gundlach, and T. N. Jackson, “Temperature-independent transport in high-mobility pentacene transistors”, *Appl. Phys. Lett.*, vol. **72**, pp. 1854, (1998).
- [15] W. Warta, and N. Karl, “Hot holes in naphthalene: High, electric-field-dependent mobilities”, *Phys. Rev. B*, vol. **32**, pp. 1172, (1985).
- [16] L. B. Schein, C. B. Duke, and A. R. McGhie, “Observation of the Band-Hopping Transition for Electrons in Naphthalene”, *Phys. Rev. Lett.*, vol. **40**, pp. 197, (1978).
- [17] E. A. Silinsh, A. Klimkans, S. Larsson, and V. Capek, “Molecular polaron states in polyacene crystals. Formation and transfer processes”, *Chem. Phys.*, vol. **198**, pp. 311 (1995).
- [18] L. Torsi, A. J. Lovinger, B. Crone, T. Someya, A. Dodabalapur, H. E. Katz, and A. Gelperin, “Correlation between Oligothiophene Thin Film Transistor Morphology and Vapor Responses” *J. Phys. Chem. B*, vol.**106**, pp. 12594,

(2002)

- [19] Liang Wang, Daniel Fine, and Ananth Dodabalapur, "Nanoscale chemical sensor based on organic thin-film transistors." *Appl. Phys. Lett.* vol. **85**, pp. 26, (2004).
- [20] Zheng-Tao Zhu, Jeffrey T. Mason, Rüdiger Dieckmann, and George G. Malliaras, "Humidity sensors based on pentacene thin-film transistors" *Appl. Phys. Lett.* vol. **81**, pp. 24, (2002).
- [21] Dawen Li, Evert-Jan Borkent, Robert Nortrup, Hyunsik Moon, Howard Katz, and Zhenan Bao, "Humidity effect on electrical performance of organic thin-film transistors" *Appl. Phys. Lett.* vol. **86**, pp. 042105, (2005).
- [22] Richard D. Yang, T. Gredig, Corneliu N. Colesniuc, Jeongwon Park, Ivan K. Schuller, William C. Trogler, and Andrew C. Kummel, "Ultrathin organic transistors for chemical sensing" *Appl. Phys. Lett.* vol. **90**, pp. 263506, (2007).
- [23] Mingxiang Wang and Man Wong, "An Effective Channel Mobility-Based Analytical On-Current Model for Polycrystalline Silicon Thin-Film Transistors" *IEEE TRANSACTIONS ON ELECTRON DEVICES*, VOL. **54**, pp. 4 (2007).

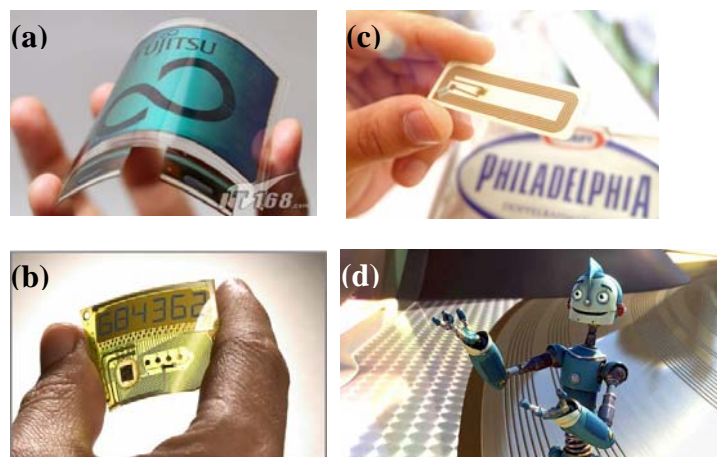


Figure 1.1 The applications of plastic transistors: (a) flexible displays, (b) smart cards, (c) RFID tags, and (d) the nervous system of robot skin. [Adapted from <http://tech.sina.com.cn/digi/2006-04-20/1204911539.shtml>]

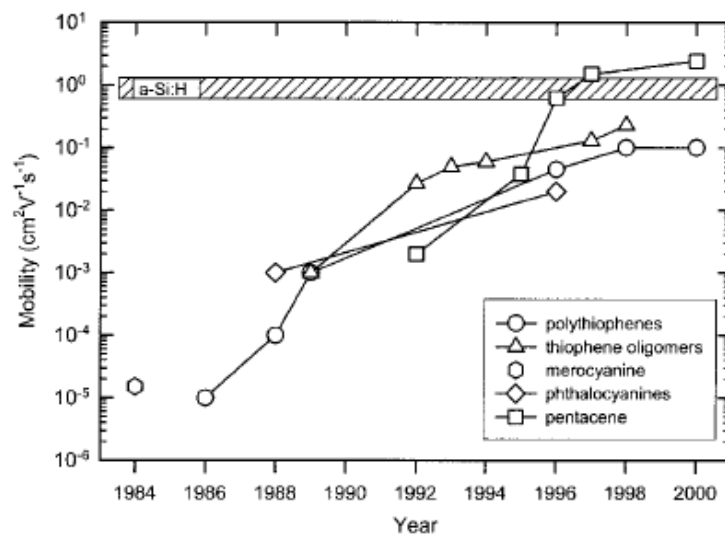


Figure 1.2 Evolution of hole mobility for the most common p-type organic semiconductors [2].

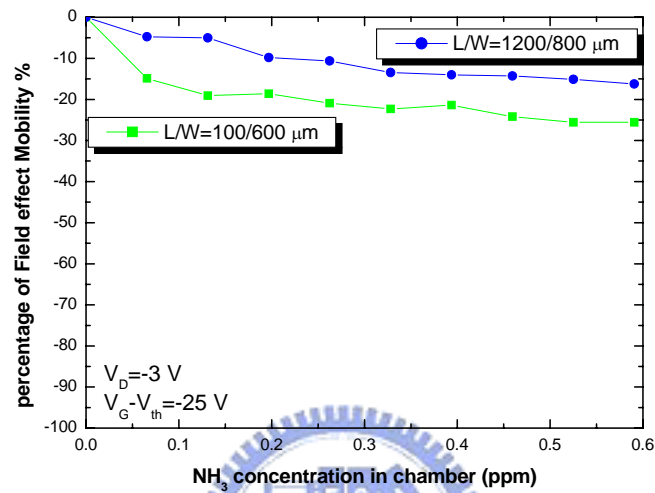


Figure 2.1 The degradation of field-effect mobility from two OTFTs with different channel dimensions.

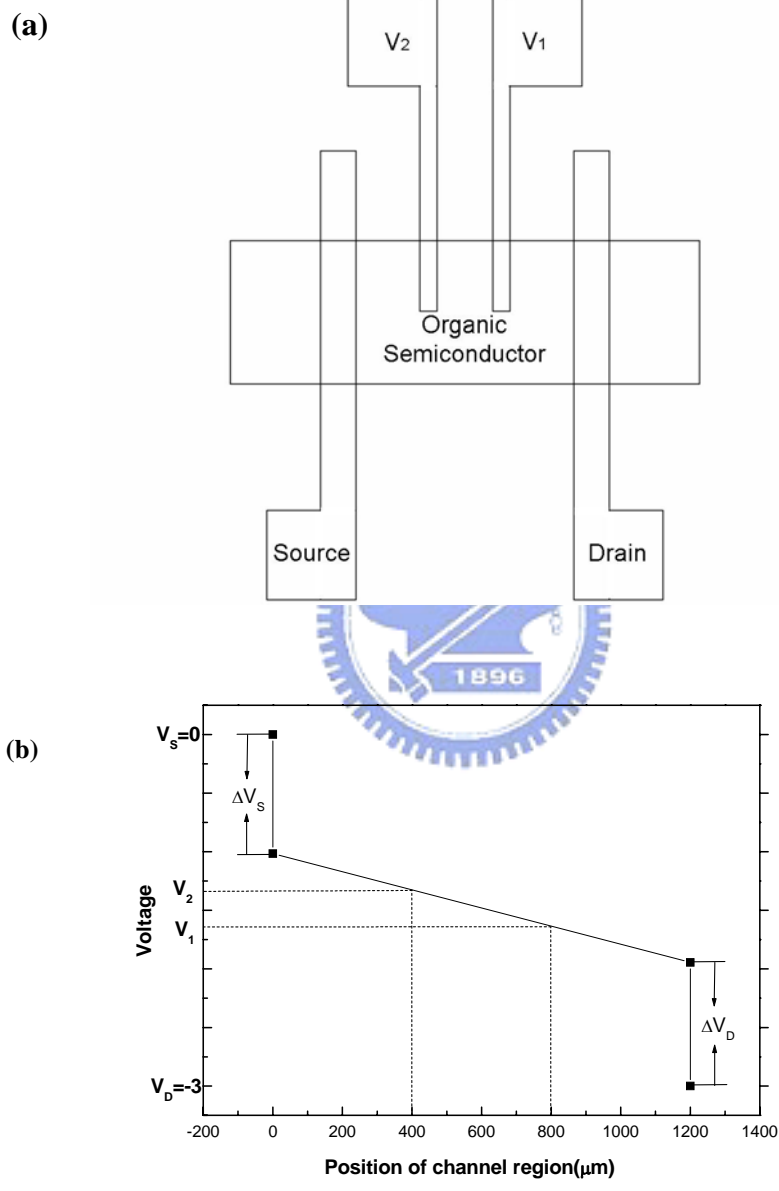


Figure 2-2. (a) Top view of a gated-four-probes OTFT. (b) The potential distribution in an OTFT channel region. The potential drop of the organic film is assumed to be

linear. But the potential different at the source and drain electrodes are also given.

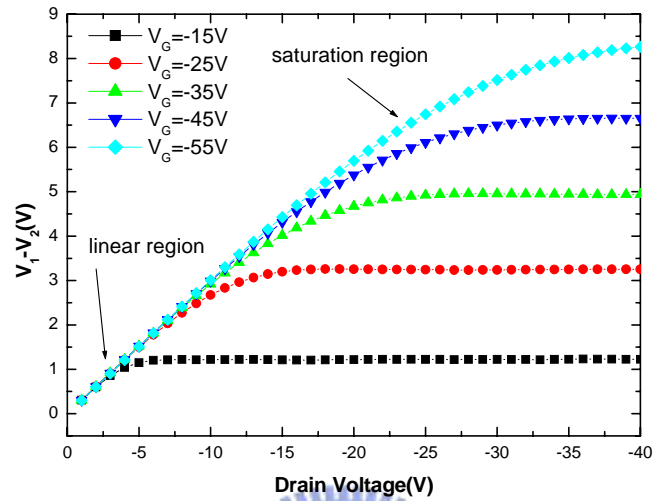


Figure 2.3 The voltage difference between two voltage probes $V_1 - V_2$ are plotted as a function of drain voltage at different gate voltage.

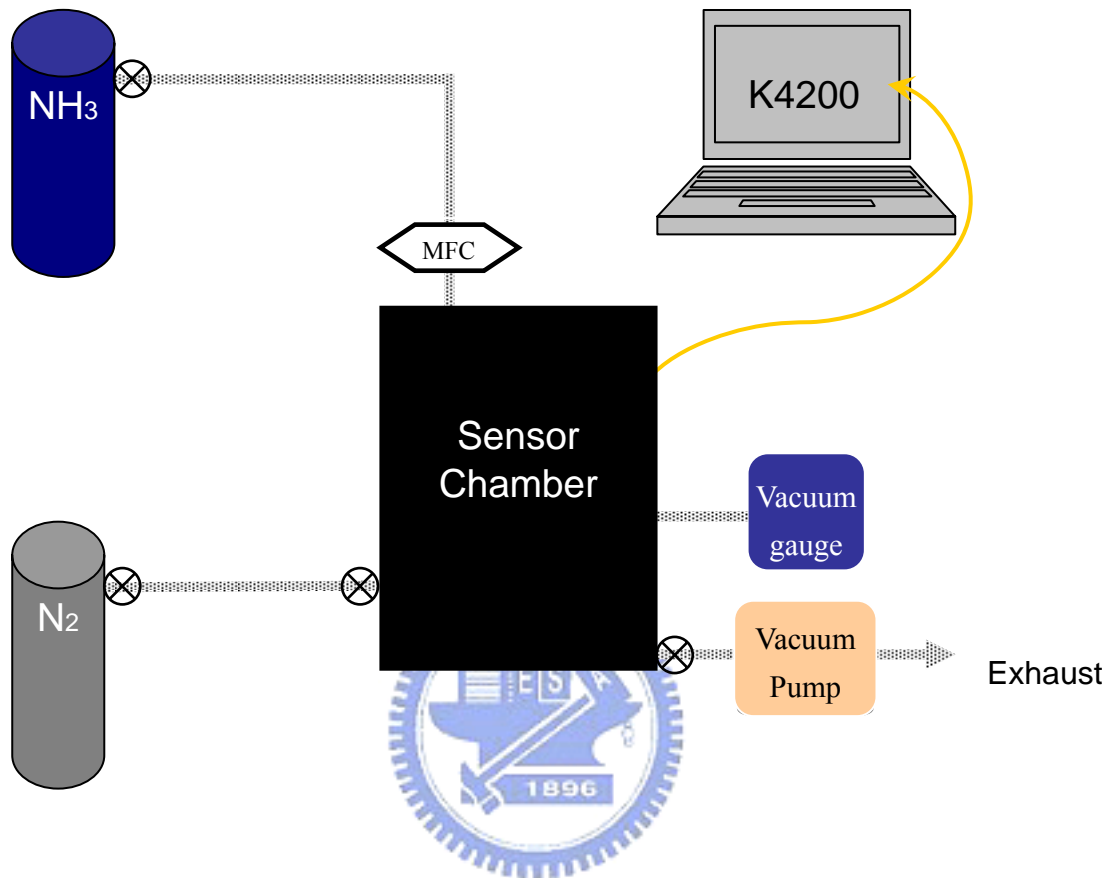


Figure 3.1 Diagram of gas sensing measurement system





Figure 3.2 (a) The mass flow controller of gas sensing system. (b) The power supply of mass flow controller. (c) The pressure gauge of gas sensing system.

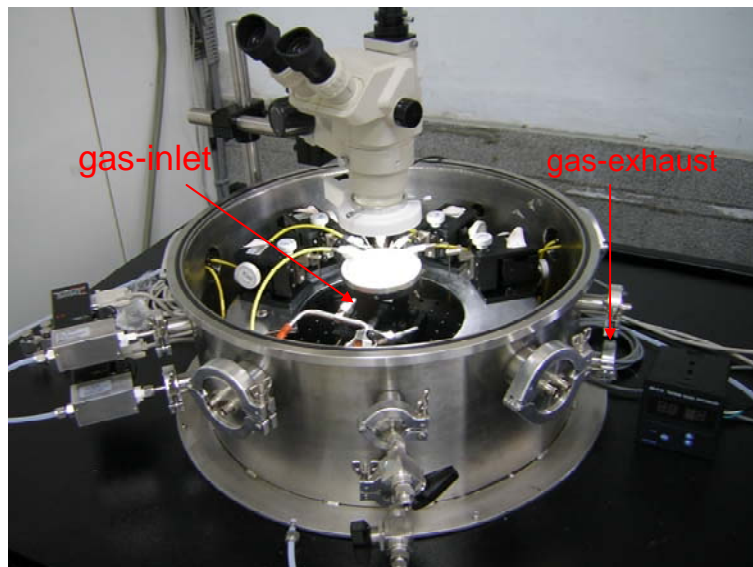


Figure 3.3 Top-view image of gas-sensing system.



Figure 3.4 Top-view image of gas-sensing system mounting a metal cap with transparent window.

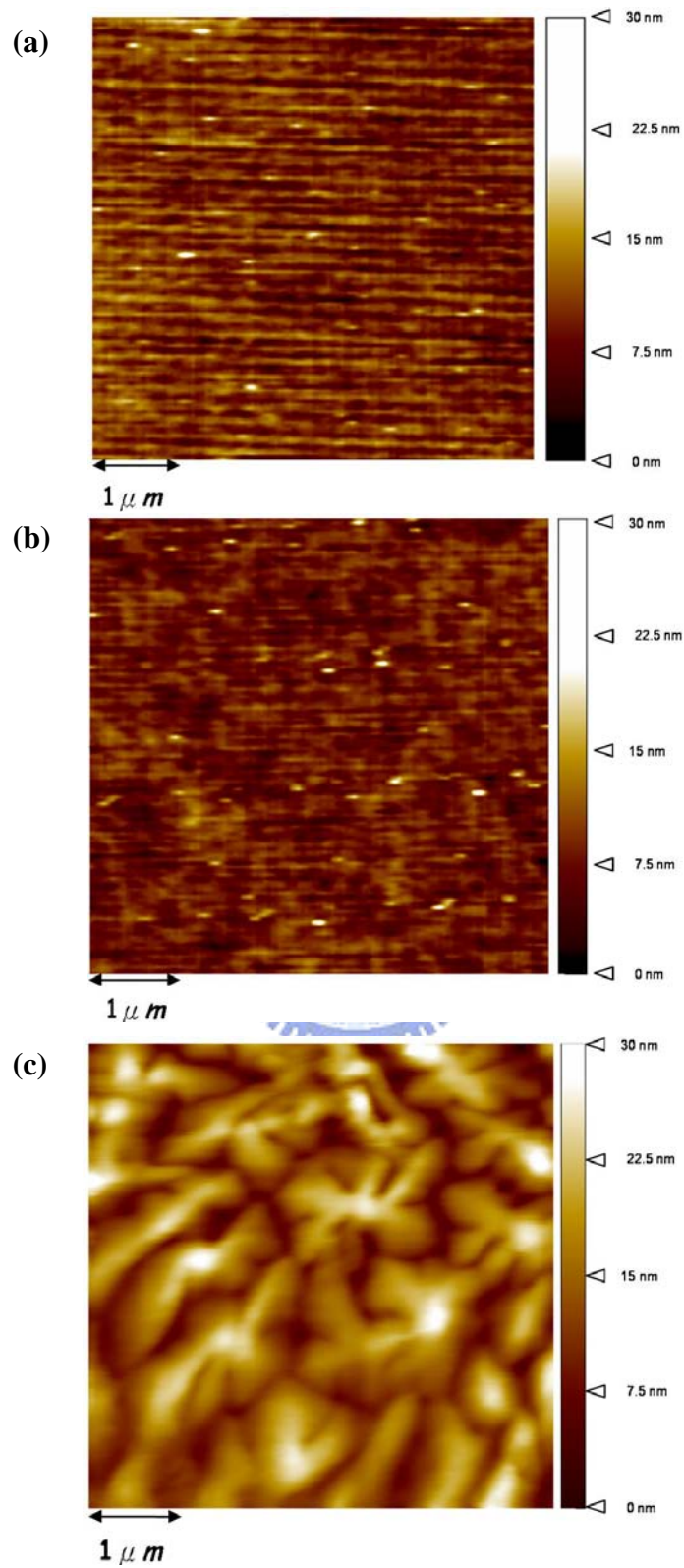


Figure 4.1 The atomic force microscope (AFM) images of (a) SiO_2 dielectric. (b) PMMA-coated SiO_2 dielectric. (c) pentacene AFM image on PMMA-coated SiO_2 layer.

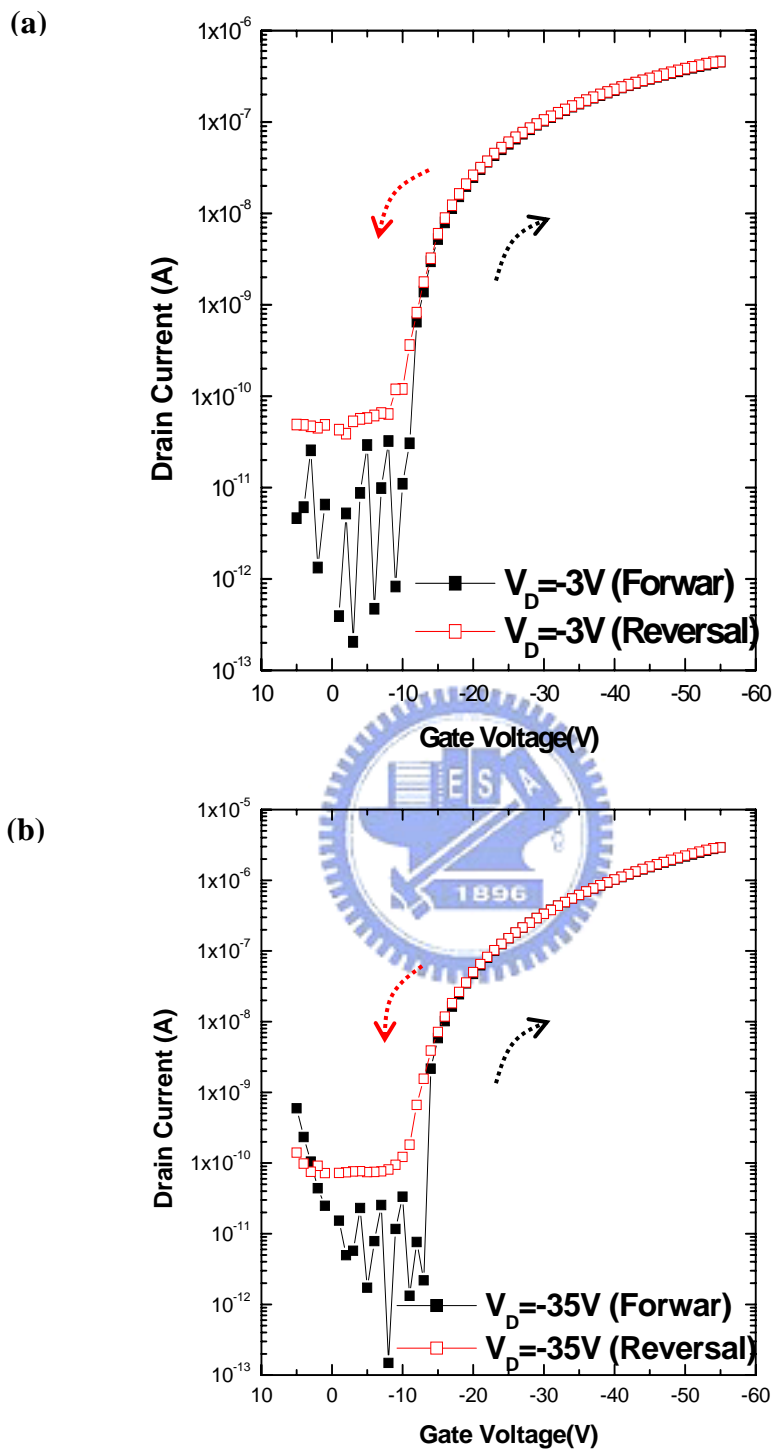


Figure 4.2 The drain-current is plotted as a function of gate-voltage. (a) Device is operated at linear region. (b) Device is operated at saturation region.

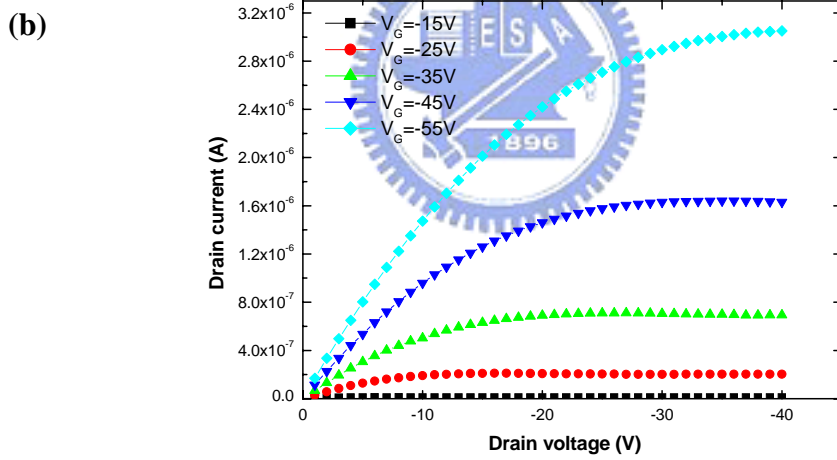
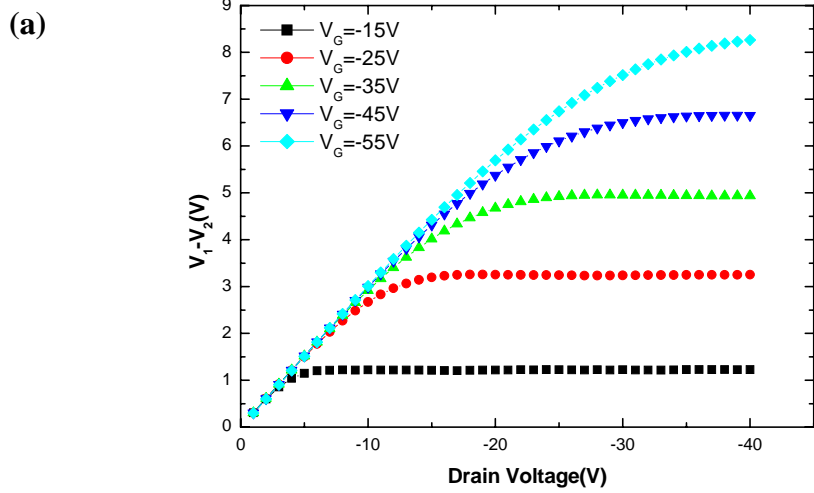


Figure 4.3 (a) The voltage difference between potential-probes is plotted as a function of drain voltage, at different gate voltages respectively. (b) The output characteristics ($I_D - V_D$) show that when V_D increases, the $I_D - V_D$ curve will be converted from a linear-relation to a saturated-relation.

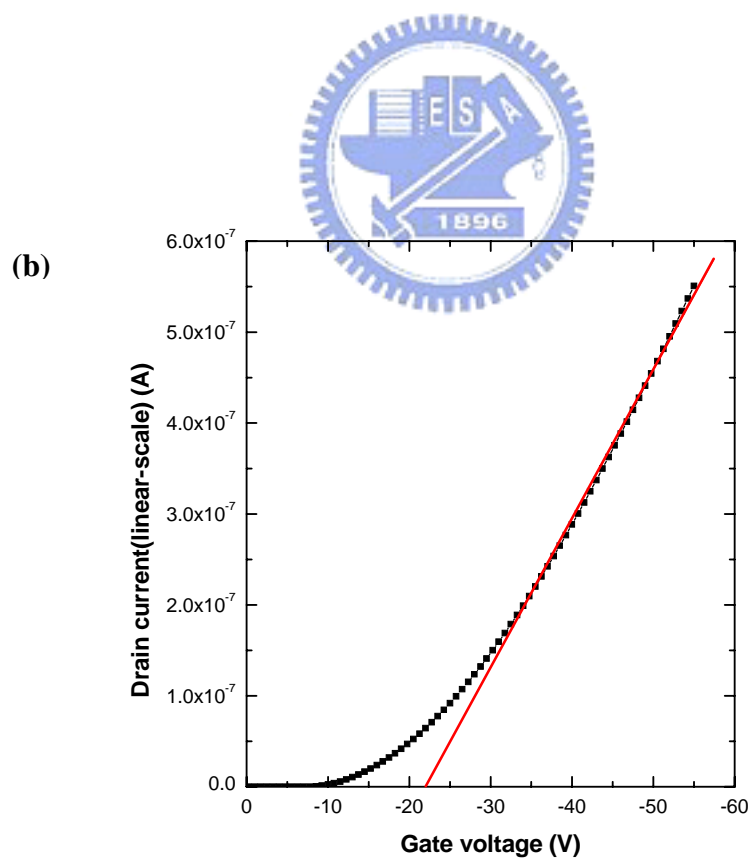
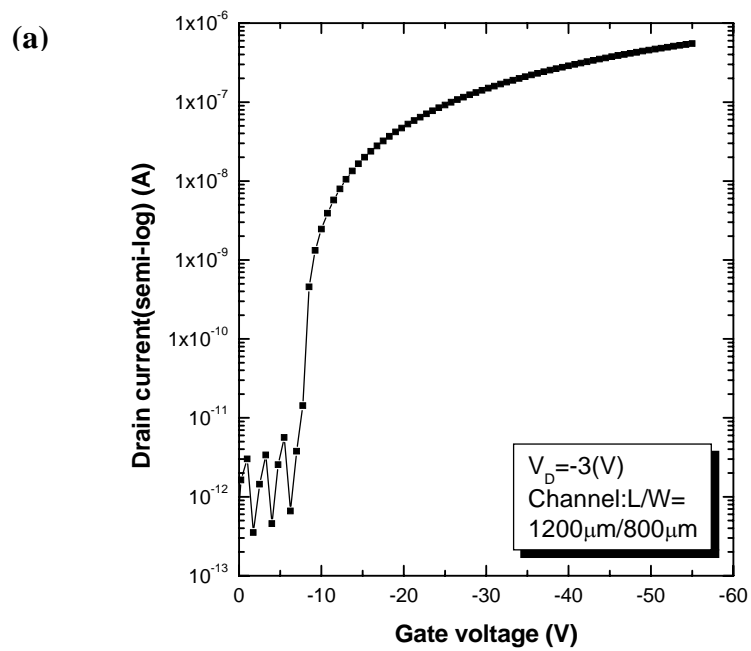


Figure 4.4 The transfer characteristic of gate-four-probes OTFT is plotted in (a) semi-log scale and (b) linear-scale, respectively.

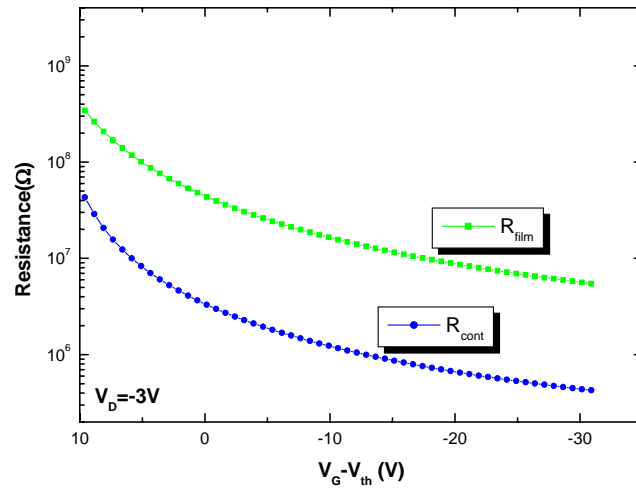


Figure. 4-5 The total contact resistance(R_{cont}) and the pentacene film resistance (R_{film}) is plotted as a function of gate-voltage minus threshold-voltage ($V_G - V_{th}$), respectively.



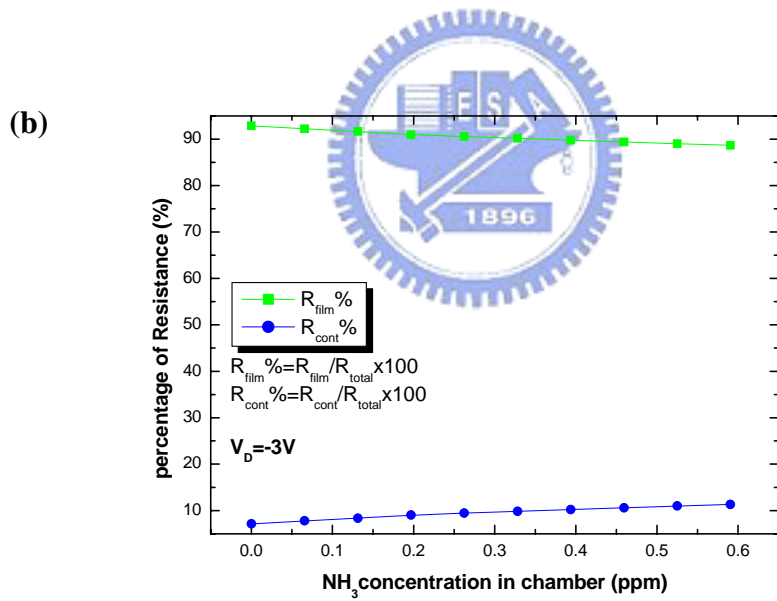
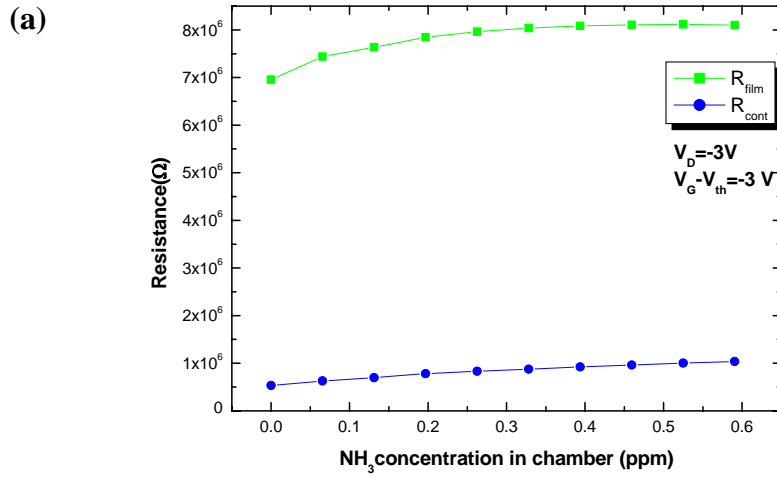


Figure. 4-6 (a) The R_{cont} and R_{film} is further plotted as a function of NH_3 concentration. (b) The percentage (%) of R_{cont} and R_{film} versus NH_3 concentration.

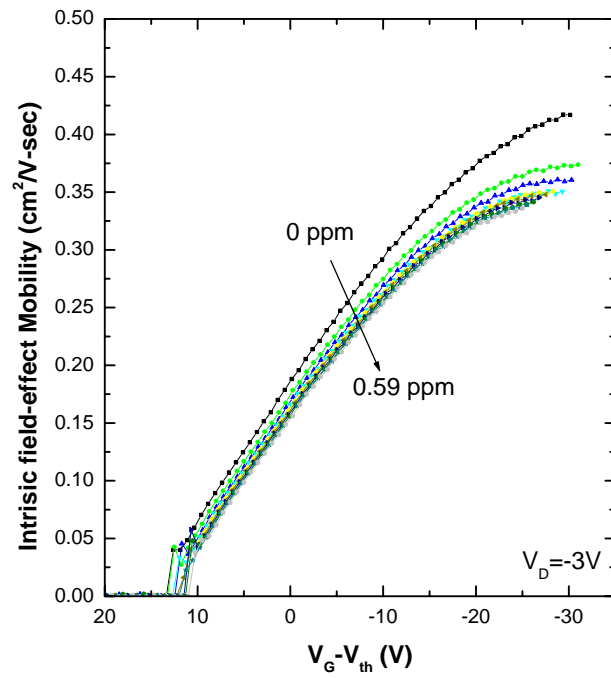
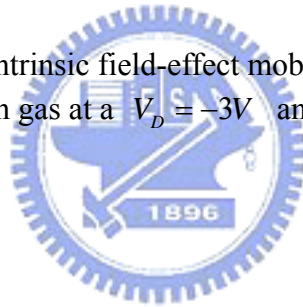


Figure. 4-7 The extracted ontrinsic field-effect mobility is plotted as a function of NH₃ concentration gas at a $V_D = -3V$ and $V_G - V_{th} = -25V$.



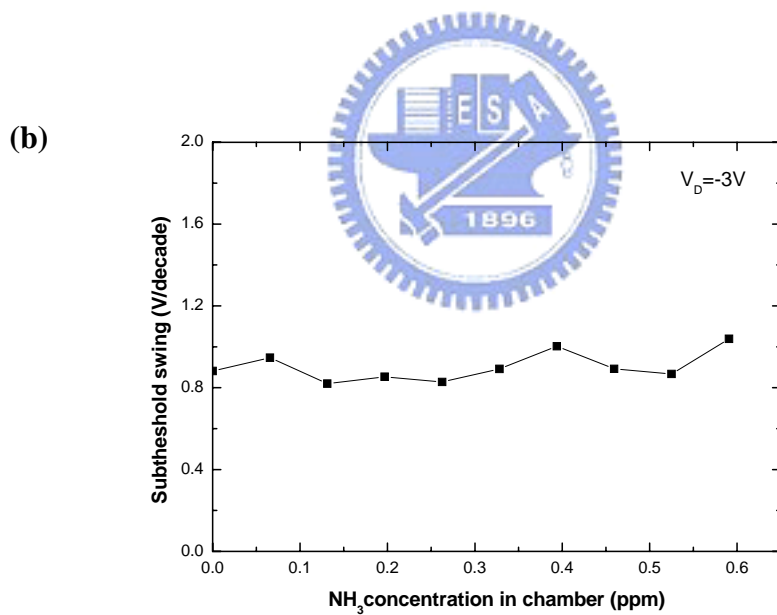
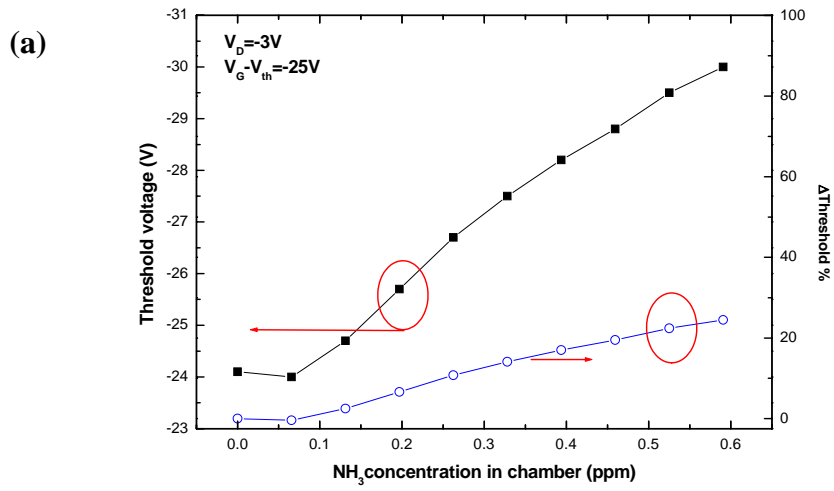


Figure. 4-8 (a) The threshold voltage shift (ΔV_{th}) and (b) the subthreshold swing ($S.S.$) is also plotted as a function of NH_3 concentration, respectively.

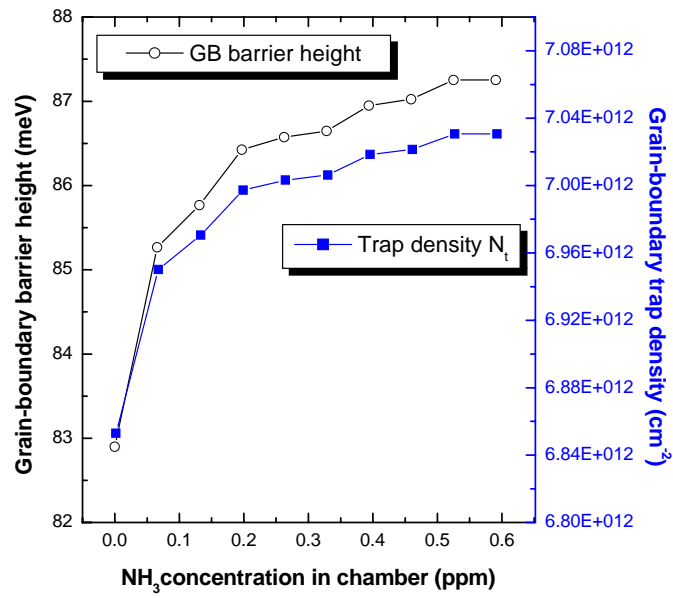


Figure. 4-9 The estimated GB barrier height and GB trap density is plotted as a function of NH₃ concentration.



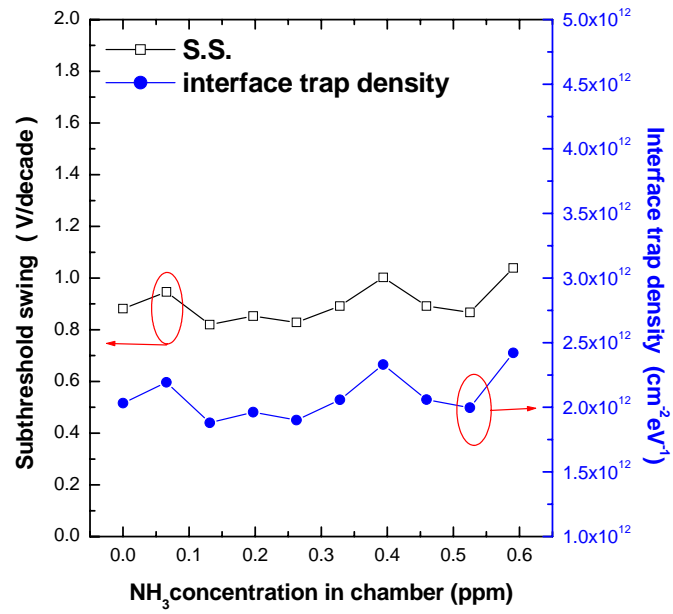


Figure. 4-10 The subthreshold swing and interface trap density will not be influenced significantly after the pentacene film interacts with the NH₃ molecular.

簡 歷

姓名：吳文馨

出生日期： 中華民國七十一年十月二十五日 (1982.10.25)

地址：屏東縣潮州鎮朝昇路 372 巷 1 號

學歷：

南台科技大學電機系學士

(2001.09-2005.06)

國立交通大學電機學院 光電顯示科技產業研發班

(2005.09-2007.08)

論文題目：

四點探針有機薄膜電晶體之氣體感測研究

Study of Gas Sensing Ability on Gated-Four-Probes

Organic Thin Film Transistors.

